Journal of Food Chemistry & Nanotechnology

https://doi.org/10.17756/jfcn.2020-099

Research Article

Open Access

Self-assembled Imprinted Polymer Film-Based Sensor System for Spermidine on Screen Printed Electrodes

Yu-Jie Huang†, Rui Chang† and Qiu-Jin Zhu*

School of Liquor and Food Engineering, Guizhou University, Guiyang, 550025, China

***Correspondence to:**
Qiu-Jin Zhu
School of Liquor and Food Engineering,
Guizhou University, Guiyang, 550025, China
Tel: 0851-88236702
E-mail: ls.qjzhu@gzu.edu.cn

Received: July 24, 2020
Accepted: October 01, 2020
Published: October 04, 2020

Citation: Huang YJ, Chang R, Zhu QJ. 2020. Self-assembled Imprinted Polymer Film-Based Sensor System for Spermidine on Screen Printed Electrodes. *J Food Chem Nanotechnol* 6(4): 174-181.

Published by United Scientific Group

Abstract

Spermidine (SPD) is an important signal molecule relate to protein food safety, but vulnerable to interference during detection. Here, an electrochemical sensor system for the spermidine detection was developed by a self-assembled molecularly imprinted polymer (MIP) film coated on disposable screen-printed electrodes. The modification imprinted polymer was prepared with template molecules SPD and functional monomer meth acrylic acid (MA) with molar ratio 1:4 through ultraviolet polymerization. The cyclic and differential pulse voltammetry (CV and DPV) scanning showed that the best adsorption equilibrium time of the modified electrodes was 360 s. The electrodes exhibited good linear relationship ranging from 1.0×10^{-6} mol/L to 5.0×10^{-6} mol/L ($y = -1.22x+7.82$, $R^2 = 0.9952$), and the detection limit was 1.7016×10^{-7} mol/L. When take high concentration of histamine and tyramine as interfering components, the modified electrodes detection relative standard deviation was < 5% and thus proved good anti-interference ability. In addition, the density function theory (DFT) calculation explored the intera-molecular interaction of SPD-MA imprinted complex, and the simulation showed that the prepared device can keep recognition stability under the potential difference stress range from 0 to 0.005 a.u. Therefore, the prepared system has the potential for rapid detection spermidine in the place.

Keywords

Spermidine, Molecular imprinting, Modified electrode, Screen-printed, Detection

Introduction

Spermidine (SPD) was biosynthesized by putrescine and methionine *in vivo* [1], which involved multifunction in life activities, promotes cell growth and lower blood pressure. It was widely present in a variety of foods (e.g., ripe cheese, pulses, mushrooms, and whole grains) [2-4], and Figure 1 shows structure schematic. *In vivo*, spermidine act as physiological blockers of inward rectifier K+ channels [5], increase autophagy-related gene transcription to expand the lifespan of model creatures [6, 7]. More importantly, as a common biogenic amine, spermidine related many to food safety [8]. The spermidine levels in meat products can reflect the freshness and spoilage degrees [9, 10], microbe species and count [11]. During food processing, the nitrite compounds in meat can form carcinogenic nitrosamines with spermidine [12]. Many studies provide that spermidine accumulated in rats has subacute toxicity (600 mg/Kg) and a strong stimulating effect on the mucosa [13], and high concentration of spermidine

in the patient body fluids related to various cancer potential [14]. Hence, the accurate and rapid detection of spermidine concentration in vitro and in vivo samples is necessary.

At present, the biogenic amines detection strategies including gas chromatography (GC), thin layer chromatography (TLC), ultra-high-performance liquid chromatography (UHPLC), ion chromatography, mass spectrometry (MS), and optical sensors [15-19]. However, most of these methods have disadvantages in rapid detection in place. Electrochemical sensors with the advantage of efficient and convenience has applied to trace food risk substance detection, which transform the concentration response changes into sensitive and sharp electrical signals. The advanced electrochemical techniques, such as Au or carbon nanoparticle-modified electrodes, pulsed amperometric detection, capillary electrophoresis electrochemiluminescence [20, 21]. And the latest methods such as the carbon dots (CDs), fluorescent sensor, smart visual detection and enzymatic biosensors [22-24]. However, these methods were insufficient to recognition target substance specificity [25]. The molecularly imprinted polymer (MIP), which can specifically adsorb target molecules, was obtained by the polymerization between the template molecule and functional monomer with the aid of a crosslinking agent [26]. And there exist many MIP modified electrode sensor devices, such as carbon electrode [27, 28], functioned graphene electrode [29], coated silica [30]. But these sensor systems also have the shortage of rapid synthesis efficiency. Screen printing is a kind of stencil printing, "probe molecules" can transfer to the substrate "holes" under pressure, the electric probe can induce oxidation reduction reaction and current change on the electrode surface. Screen printed imprint modified electrode was widely used in many rapid detection fields [31].

In order to improve the spermidine detection above, we prepared a disposable biosensor based on the screen-printed electrodes, the electrodes modified with imprinted polymer can specific identification spermidine in the presence of interferences. The polymer was directly polymerized on the electrode surface with functional monomer meth acrylic acid assist by the crosslinking agent ethylene glycol dimethacrylate, and the electron acceptor $K_3[Fe(CN)_6]$ was used as a typically probe substance because it was a good electrical conductor. Moreover, considered the potential difference occurs periodically at the electrode cyclic voltammetry detection response process [32, 33], and the induced electric field effect may impact the structural stability of the imprinted complex, the density function theory (DFT) calculation was used for electronic structure parameters and intra-molecular weak interaction analysis. Over all, our work can provide a certain reference for the preparation of spermidine rapid detection devices (Figure 1).

Materials and Methods

Reagents and instruments

Spermidine and histamine (purity 98%; Sigma-Aldrich, USA), tyramide and meth acrylic acid (purity 99%; Sigma-Aldrich, USA), ethylene glycol dimethacrylate (purity 98%; Sigma-Aldrich, USA), azobisisobutyronitrile (analytical grade; Chengdu Gresia Chemical Technology Co., Ltd. China), potassium ferricyanide (analytical grade; Tianjin Kemico Chemical Reagent Co., Ltd. China), nitrogen (Guizhou Yong-sheng Industrial Gas Company, China), and screen printing electrode (Kim Kun Biological Engineering Co., Ltd., Wuxi City, China).

WYH-2 water bath oscillator (Jintan Jing-da Instrument Manufacturing Co., Ltd.China), HH-W420 constant temperature water bath (Xing-tai Runlian Machinery Co., Ltd. China), SB-100D ultrasonic cleaner (Ningbo Xinzhi Biotechnology Co., Ltd. China), FA2004B electronic analysis balance (Shanghai Velvet Instrument Co., Ltd. China), and CHI604E electrochemical workstation (Shanghai Chen Hua Instrument Co., Ltd. China).

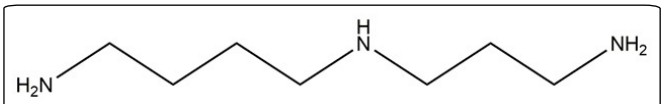

Figure 1: Schematic of spermidine structure.

Methods

Screen printed electrodes pretreatment

The electrode was first immersed at 20% H_2O_2 solutions for 20 min and then at 20% H_2SO_4 for 20 min to clean the dust and oxidation on the surface. Then, the electrode was continuously soaked with deionized water for 20 min, and then dried and preserved at 4°C for further use.

Electrodes buffer preparation

The $K_3[Fe(CN)_6]$ phosphate buffer solution with the concentration of 0.5 mmol/L and pH of 7.0 was prepared using 1.646 g potassium ferricyanide standard and 0.2 mol/l phosphate buffer. The 0.2 mol/L phosphate buffer solution was prepared by adding 39 ml of 0.2 mol/L NaH_2PO_4 and 61 mL of 0.2 mol/L Na_2HPO_4 in a beaker.

Spermidine molecularly imprinted polymer film preparation

Based on our previous work [34], choose the theory calculated optimum molar ratio of template molecules spermidine to the functional monomer methacrylic acid 1:4 as the experimental polymerization ratio. Accurately weighed 217.5 mg spermidine and 100 mg azobisisobutyronitrile, accurately measured 510 mL of meth acrylic acid and 2 mL of ethylene glycol dimethacrylate, mixed in a beaker. Then, 50 mL of carbon tetrachloride solution were added, and the solution was placed in 100 W ultrasonic cleaners for dissolution, nitrogen was bubbled to remove dissolved oxygen within the solution system. For polymerization, take 1.5 μL polymerization solution and dropped into the working area of the screen-printed electrode covered with cover glass to isolate oxygen and form a uniform film. Note that the cover glass should be used for covering to ensure that the polymerization solution cover the reference electrode and prevent impact, and the entire dropping and glass slide covering steps must be performed as quickly as possible to avoid rapid evaporation of carbon tetrachloride. Then, placed modified electrode in an incubator at 4 °C and irradiated with 365 nm UV lamp at a distance of < 10 cm to polymerization for 96 h. After

polymerization was completed, a waxy surface layer was formed on the electrode surface. The prepared modified electrodes were stored at 4 °C for next steps.

Spermidine-imprinted modified electrode elution time

The prepared spermidine-imprinted electrode was soaked into 10% methanol acetic acid solution (v/v = 9:1), and stirred gradually for elution spermidine molecules. In order to avoid excessive elution MIP layer, the stirring intensity should not be too strong. The DPV scanning method was used every 60 s after 60 s of elution in the range of -0.6 V~0.8 V.

Spermidine-imprinted modified electrode adsorption time

Equilibrium adsorption time can reflect the electrode detection speed. The specific adsorption of spermidine on imprinted modified membrane electrodes was dynamic adsorption equilibrium process through intermolecular weak intermolecular interactions [35]. The spermidine-imprinted modified electrode was placed into the buffer solution for adsorption test, and the adsorption time interval was 60 s. After adsorption, the spermidine remaining on the surface was washed with distilled water. Then, the electrode was inserted into the spermidine-free buffer to perform DPV scan at range of –0.8~1.0 V, record the peak current and plot it versus time.

Spermidine-imprinted modified electrode detection limit

The lower detection limit of the electrode, the more detection sensitivity of the electrode. After elution, the imprinted modified electrodes were placed in adsorption solution at series concentration 1, 2, 3, 4, 5 μmol/L. The saturated adsorption time was referenced with the adsorption equilibrium time (360 s), and the current changed was detected by DPV scanning in the range of –0.8~1.0 V. Plot the standard curve with the response values and spermidine concentration. The detection limit was determined by formula: DL = 3δb/K, where δb is the standard deviation (SD) of blank parallel determination (10 times) and the calculated values, and K is the slope of the standard curve [36].

Interference experiment

Molecularly imprinted polymers can adsorb the target substance by geometric and structural matching principles [36]. Tyramine and histamine, similar in shapes and groups of spermine, were selected as interfering components. First, a buffer solution containing 1.0 × 10–6 mol/L SPD was prepared in 2 beakers, and 50-fold molar tyramine and histamine concentrations were added. The eluted spermidine imprinted polymer modified electrode was placed in a beaker for adsorption. The adsorption time was referenced with the adsorption equilibrium time. For check the occupied conditions of eluted holes on SPD, after adsorption was completed, the buffer solution was subjected to DPV scanning, and the results were compared with the current changes.

DFT theory calculations

The DFT calculation was used to simulation and explore the electrode modification material molecular imprinted complex (SPD and MA with best polymerization ratio 1:4) structural stability under the external electric field. The geometry optimization with frequency vibration analysis of the SPD-MA complex were performed on the B3LYP/6-311G (d, p) theory level at gas phase, and the keywords nosymn fixed the SPD-MA complex oriented at the external electric filed direction. The external electric field was set at SPD-MA complex cartesian coordinates X axis with intensity values 0, 0.001, 0.002, 0.003, 0.004, 0.005 a.u (1.a.u = 51.423V/angstrom), which range from 0V/angstrom to 0.25V/ angstrom. The single point energy was calculated at M062X/def2TZVP level based on the optimized structure with on imaginary frequency. For thermodynamics data, the vibrational zero-point energies (ZPEs) scale factors was 0.988.

Bader's Atoms in Molecules (AIM) theory states that the electron density distribution is related to the chemical bond type. The bond critical point (BCP) occurs between attractive atom pairs, the most important was hydrogen bond donor and acceptor atoms. For small interacting monomers, the strength of hydrogen bonds (EHB) can be reasonable characterized by binding energies (BEs). And the BEs of neutral hydrogen bond has the fitted equation with electron density at the corresponding bond critical point (BCP).

$$BE \approx -223.08 \times \rho(BCP) + 0.7423 \quad (1)$$

where the unit of ρ is a.u., the unit of BE is kcal/mol [37].

In order to visualization the inter-molecular weak interactions at SPD-MA complex BCPs, the independent Gradient Model (IGM) for non-covalent interaction (NCI) analysis was also performed. All the DFT theory calculations were performed on the Gaussian 16 (Revision A. 03) package support by the Guizhou University High performance computing cluster [38]. The BCP and IGM analysis of SPD-MA complex was finished by Multiwfn 3.8 suites on the personal computer [39].

Results and discussion

Spermidine-imprinted modified electrode elution time and stability

When elution imprinted polymers with buffer solution, it generated "holes" that allow the probe electric substance pass through. When detection, the film-modified electrode absorbed spermidine immediately and blocked the "holes", thus the probe $K_3[Fe(CN)_6]$ cannot pass through [40]. The electrode elution was at 10% methanol acetic acid solution (v/v = 9:1). In order to measure the current changes of the modified electrode elution process, the DPV scan was performed at the scan range of -0.8 ~1.0 V, the result is shown in figure 2.

The stability of modified electrode was also crucial to the subsequence results. Many studies show that the electrode surface was not absolutely smooth [41], thus make the MIP films coated on the surface tightly during the UV polymerization process. Furthermore, after elution, a three-dimensional network porous structure formed on the MIP modified electrode surface. And the network porous, which cross-linked each other and adhered to the rough electrode surface through molecular force interaction [42]. The electrode potential stability of the bare electrode, eluted electrode, un-

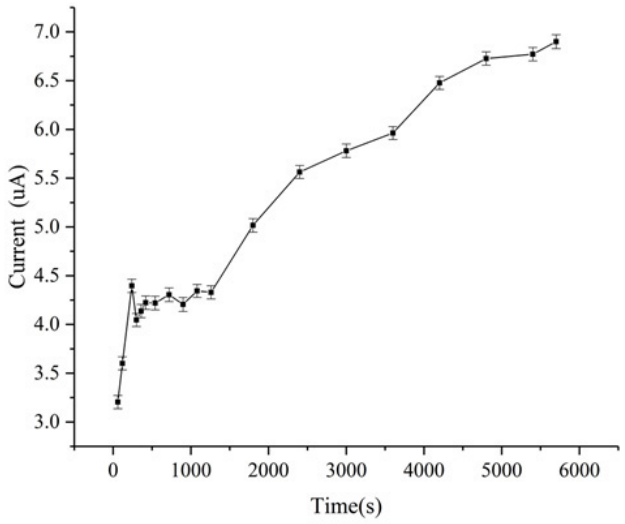

Figure 2: Elution time of the imprinted modified electrodes.

eluted electrode in buffer solution (contain the probe substance $K_3[Fe(CN)_6]$) was also measured at the same conditions by CV scan, and the result was at figure 3.

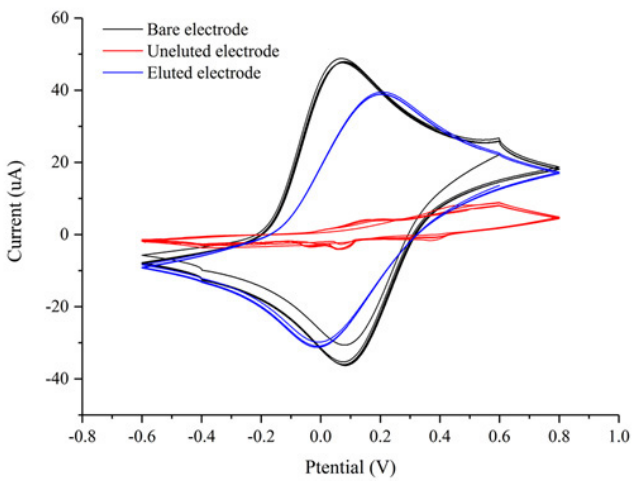

Figure 3: CV scan of the three electrodes (Bare electrode, Uneluted electrode, Eluted electrode).

As shown in figure 2, the response current was only almost 3.0 μA at the begin of elution. In this imprinting stage, the polymer film was assembled on the electrode surface, and the spermidine wrapped in the pores that formed by the functional monomer and crosslinking agent. Only few holes present on the electrode surface were still open, thus make probe substance $K_3[Fe(CN)_6]$ cannot pass through because eluted cavities were occupied by spermidine molecules, and the electrodes cannot specifically detect spermidine because the current transportation pathway was obstructed. When eluted the template molecular spermidine, the movable $K_3[Fe(CN)_6]$ probe and the electrode surface process redox reaction and exhibited electrical signals. From figure 2, As the elution time increase, the current upped significantly from 1000 s to 4000 s, indicated the spermidine was gradually eluted from the pores. During the stage, the imprinted modified electrodes also can adsorption spermidine from the mixed solution by specific recognition ability, and the reabsorbed spermidine molecules binding the pores against with the $K_3[Fe(CN)_6]$ molecule to keep a dynamic equilibrium. Given that spermidine was not electrostatic substance, the current flow generated on the electrode surface is reduced [43]. As shown in figure 2, the increased current tends to stabilize at 4200 s, which may point to the end of elution. Considered that the current of the entire system ranging from 4200 s to 5700 s only increased 0.2 μA, the elution termination time was set at 4200 s.

In figure 3, bare electrodes possessed the largest scan peak because the surface was uncovered with the imprinted polymer, and the $K_3[Fe(CN)_6]$ in solution contacted abundantly on the electrode surface. When the electrode work area surface was covered by molecularly imprinted polymer, the un-eluted polymer blocked the pores by spermidine on the electrode surface. Hence, $K_3[Fe(CN)_6]$ cannot contact the electrode surface to undergo redox reaction and electron transfer, causing the smallest peak current generated. The peak current of the eluted electrode was smaller than the bare electrode because the imprinted polymer itself coated on the electrode working area. In above, the electrode peak current sequence satisfied: bare electrode > eluted electrode > un-eluted electrode. This illustrated that the un-eluted electrode passed through the smallest amount of $K_3[Fe(CN)_6]$, and the eluted electrode passing through $K_3[Fe(CN)_6]$ was still smaller than the bare electrode.

Spermidine imprinted modified electrodes adsorption time

The current changes of the electrode adsorption spermidine was in figure 4. The equilibrium adsorption time of the imprinted modified electrodes on spermidine was shown in figure 5.

From figure 4, after adsorption, the current of the modified electrode was lower than before and reached maximum peak values when the potential values near zero, which indicates the adsorption status has become saturated. The spermidine concentration in the sample solution can measured by the relationship between the scanned current and the spermidine adsorption gradient concentrations. As shown in the curve in

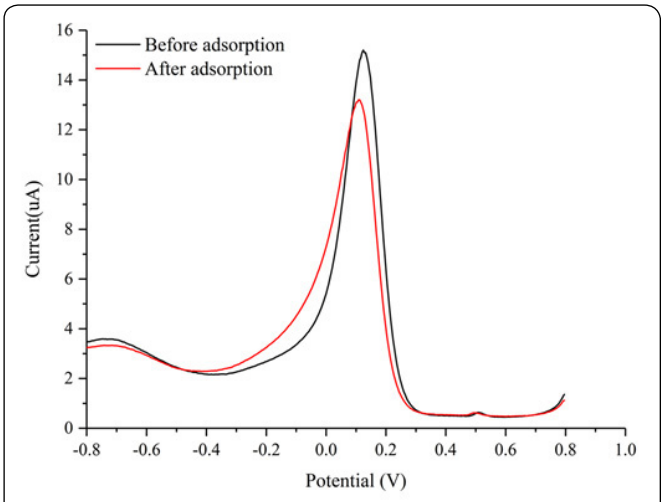

Figure 4: DPV scan of SPD imprinted modified electrodes before and after adsorption.

figure 5, at first, the current value decreased rapidly and then gradually increased until reached equilibrium. This indicated that the nonspecific adsorption played an important role at the beginning of the adsorption process, and the specific adsorption occurred afterward. This was consistent to the adsorption and recognition of spermidine by molecularly imprinted polymer that at polymerization ratio of 1:4. And from figure 5, the response current value was decreasing along with the adsorption time because the spermidine molecules re-adsorbed subsequently after the probe substance $K_3[Fe(CN)_6]$ eluted from the imprinted polymer. The response current was close to equilibrium at 360 s, and in order to shorten the detection time, we defined the electrode adsorption time of spermidine sample solution as 360 s. Figure 5 shows that the current values decreased obviously after adsorption completely, this relate to the decrease of the electrode surface cavities and the amount of moveable $K_3[Fe(CN)_6]$.

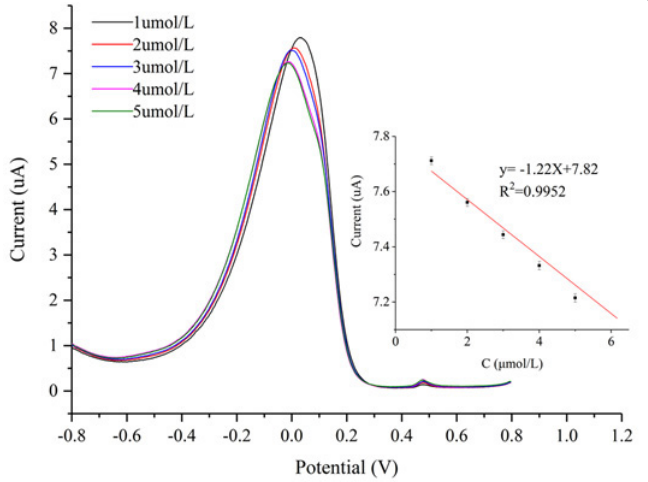

Figure 5: SPD molecularly imprinted membrane electrodes adsorption time.

Spermidine imprinted modified electrode detection limit

The detection limit (DL) of prepared electrodes was performed with a series concentration adsorption solution (1, 2, 3, 4, 5μmol/L) by DPV scan. The changes of the electrode response current with concentration was show in figure 6. The relationship curve of the current and concentration was in figure 6 sub figure. The linear equation was as follows: y = −1.22x+7.82, R^2 = 0.9952. The detection limit was calculated by using the following equation: DL = 3δb/K, and get the electrode detection limit values 0.17016 μmol/L. From figure 6, when the concentration > 5 μmol/L, the current changes not keep reduced because molecularly imprinted polymer film almost reached saturation adsorption at this time. The adsorption capacity cannot increase with the adsorption solution concentration. Therefore, the prepared electrodes possessed a good linearity ranging 1.0 × 10^{-6} mol/L to 5.0 × 10^{-6} mol/L with the detection limit of 1.7016 × 10^{-7} mol/L. Similarly, the MIP modified carbon paste (CP) histamine detection electrode with meth acrylic acid and acetonitrile as porogens, shows the maximum linear response ranges was 7 × 10^{-7} mol/L [44]. By contrast, the histamine detection limitation in canned tuna through molecularly imprinted polymers-surface enhanced Raman spectroscopy was 10^{-5} mol/L [45]. The U.S. Food and Drug Administration set histamine limits in food in general at 4 × 10^{-4} mol/L [46], considered the convenient polymerization method and lower cost, our prepared electrode can be used to detection food spermidine content.

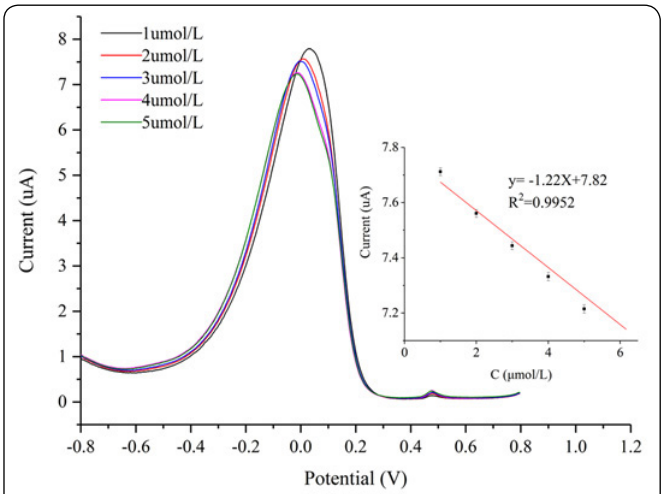

Figure 6: DPV scan of the SPD molecularly imprinted membrane electrode detection limit. (Sub figure for the calibration curve of the SPD molecularly imprinted membrane electrode).

Interference experiment

The 50-fold spermidine concentrations (50.0 × 10^{-6} mol/L) interference components tyramide and histamine were added to the buffer solution, and the solutions was scanned by DPV to obtain the current value changes. The result was shown in table 1.

Table 1 shows the relative standard deviation (RSD) was < 5%, indicated the presence of interference components effect little on the current change. As reported, the RSD of a surface plasmon resonance histamine sensor based on molecularly imprinted polymer film was range from 2.48% to 4.66% [47]. Moreover, the lowest RSD of imprinted fluorescent spermidine chemosensor at spiked serum was 3.5% [48]. Therefore, our prepared imprinted modified electrode possessed a good selective adsorption capacity for the target substance spermidine, because the eluted molecularly imprinted polymer specific adsorption sites cannot recognize the interfering substances. Hence, the interference substance cannot block the cavities. Furthermore, due to the specificity adsorption equilibrium of modified electrode only occurred on the target substance spermidine during the adsorption process. Therefore, the response current value of the interfering components group was very similar to the blank control group.

Table 1: Effect of interfering substance on SPD imprinted modified electrode.

Number	No interfering substances (μA)	With interfering substances (μA)	Relative standard deviation (%)
Spermidine/tyramine	7.71	7.85	1.83
Spermidine/histamine	7.71	7.55	2.06

Structural stability of SPD-MA imprinted complexes

As many reports shows [49, 50], the hydrogen bond binding energy ($\Delta E_{binding}$) donated the main intera-molecular weak interaction in MIP system, which was crucial for the stability of self-assembled supramolecular system. The atom in molecules (AIM) theory and independent Gradient Model (IGM) was widely used in intera-molecular non-covalent interaction (NCI) analysis. Similar to reduced density gradient function, the IGM can analyze NCI based on the electron density topology, and when define the isosurfaces as function S, there has the equation as follows [51]:

$$S = \frac{1}{2(3\pi^2)^{1/3}} \frac{|\nabla\rho(r)|}{(\rho(r))^{4/3}}$$

where ρ(r) represents the electron density (ED) and |∇ρ(r)| stands for the norm of the ED gradient vector. The basis of the Independent Gradient Model (IGM) is also ED gradient in terms of atomic components. When SIGM based on the |∇ρ(r) IGM|, the largest deviation of SIGM and S occurring at the bond critical point (BCP). Set the difference as function δg, δg(r) = |∇ρ(r)IGM|-|∇ρ(r)|. δg can divided into intramolecular interaction (δgintra) and intermolecular interaction (δginter). The figure 7 was the BCP combined IGM analysis of the SPD-MA complex, the green colours are identified as Van der Waals interaction and blue colours identified hydrogen bond.

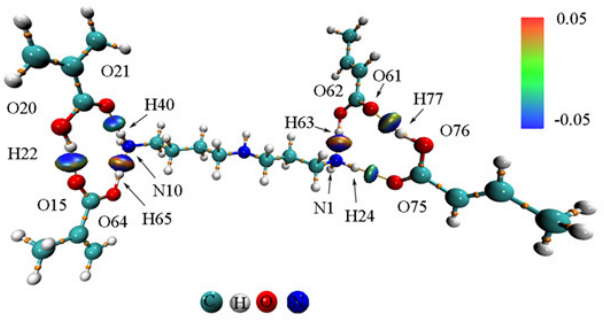

Figure 7: Non-covalent interaction (NCI) and BCP between SPD-MA complex (0 a.u, at gas phase). Bond critical points are shown as orange spheres. Bond paths are drawn as yellow paths. SPD-MA complex structure is represented as CPK model. Carbon, hydrogen, oxygen, nitrogen atoms is colored by cyan, white, red and blue, respectively. The dark blue oval region between the SPD and MA is isosurface of reduced density gradient (RDG) of 0.015 mapped by sign (λ2)ρ function.

Form the figure 7, it was clear that the SPD-MA complex with ratio 1:4 formed six hydrogen bonds at the corresponding BCP because of its abundant blue color isosurface areas.

The hydrogen bonds numbers was consistent with our previous results, which was calculated under B3LYP/6-31+(d,p) level [52]. By mapping the δg descriptor with the sign function sign (λ^2) ρ, get the SPD-MA complex non-covalent interaction scatter plot at figure 8. Form the figure 8, it can be see that the blue hydrogen bond points were more than green Van der Waals interaction points, which was consistent with the IGM isosurface analysis results.

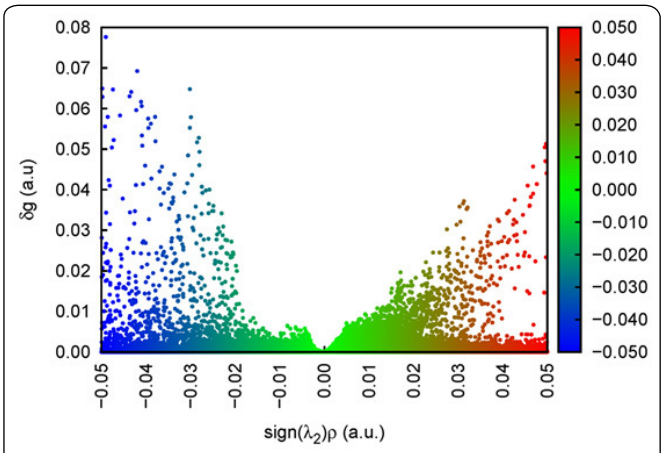

Figure 8: The scatter plot of SPD-MA complex intra-molecular interaction.

In general, the charge redistribution was related to bonding properties [53]. And the external electric field can impact the molecular structure by changing the charge distribution and molecular dipole. Combined the IGM analysis results, the intermolecular hydrogen bond at the BCP contributed most to the MIPs specific recognition ability. Therefore, we discuss focused on the hydrogen strength or binding energy here, and the results was list at table 2.

Table 2: The hydrogen bond strength (E_{HB}) of SPD-MA complex under the external electric field.

Hydrogen bond	0 a.u	0.001 a.u	0.002 a.u	0.003 a.u	0.004 a.u	0.005 a.u
O_{20}-H_{22}…O_{15}	-32.61	-32.5	-32.43	-32.54	-32.62	-32.65
O_{64}-H_{65}…N_{10}	-67.88	-65.63	-63.88	-62.6	-61.27	-59.62
N_{10}-H_{40}…O_{21}	-19.31	-19.36	-19.35	-19.14	-18.86	-18.45
O_{62}-H_{63}…N_1	-70.42	-71.74	-72.58	-73.81	-75.89	-78.23
N_1-H_{24}…O_{75}	-20.05	-19.78	-19.3	-18.42	-17.58	-16.64
O_{76}-H_{77}…O_{61}	-32.67	-33.34	-34.21	-35.31	-36.04	-36.45
Total (kJ/mol)	-242.95	-242.36	-241.76	-241.83	-242.26	-242.05

Form the table 2, all the SPD-MA molecular imprinted complex formed six hydrogen bonds under the external electric field range from 0 to 0.005 a.u. The hydrogen bond strength of O_{64}-H_{65}…N_{10}, N_{10}-H_{40}…O_{21} and N_1-H_{24}…O_{75} was little decreased with the external electric field intensity increasing. While the E_{HB} values of O_{62}-H_{63}…N_1 and O_{76}-H_{77}…O_{61} was little increased with the external electric field intensity decreasing. Compared with the 0.05 a.u results to 0 a.u outfield conditions, the E_{HB} maximum changes was 8.26 kJ/mol, which was only occupied 3.34% of total E_{HB} values at 0 a.u conditions. This indicated that electric field impact little on the SPD-MA molecular imprinted complex binding ability at the field intensity range from 0 to 0.005 a.u. Moreover, the effect of the external electric field on the whole complex system was not reasonable, because sum of the six hydrogen bonds strength was very similar at range of 0 to 0.005 a.u electric field, and the maximum changes was only 1.12 kJ/

mol. The E_{HB} analysis showed the electric field stability of our prepared molecular recognition device.

Conclusions

This study combined the molecularly imprinted modified electrode technology and the screen-printed established an electrochemical sensor for specific spermidine detection. The performance of the prepared electrodes was characterized by DPV scanning and adsorption trials, as well as elution equilibrium process. The elution equilibrium time of the template molecules spermidine was 4200 s, and the adsorption equilibrium time was 360 s. The modified electrodes possessed a good linear relationship ranging from 1.0×10^{-6} mol/L to 5.0×10^{-6} mol/L ($y = -1.22x + 7.82$, $R2 = 0.9952$), and the detection limit was 1.7016×10^{-7} mol/L. The interference components showed the modified electrodes exhibited good anti-interference ability. The DFT calculations showed that the structural stability of SPD-MA imprinted complex changes little under the external electric filed at intensity range from 0 to 0.005 a.u, which indicated the prepared device can resistant to a certain level of potential difference stress. With the advantage of convenient, stable, and sensitive, the prepared spermidine detection electrodes avoid the complex sample processing steps, and provide a reference method on protein food safety evaluation.

Conflict of Interest

The authors declare no conflict of interest.

References

1. Michael AJ. 2016. Biosynthesis of polyamines and polyamine-containing molecules. *Biochem J* 473(15): 2315-2329. https://doi.org/10.1042/bcj20160185
2. Sagara T, Fiechter G, Pachner M, Mayer HK, Vollmann J. 2017. Soybean spermidine concentration: Genetic and environmental variation of a potential 'anti-aging'constituent. *J Food Compos Anal* 56: 11-17. https://doi.org/10.1016/j.jfca.2016.11.008
3. Eisenberg T, Abdellatif M, Zimmermann A, Schroeder S, Pendl T, et al. 2017. Dietary spermidine for lowering high blood pressure. *Autophagy* 13(4): 767-769. https://doi.org/10.1080/15548627.2017.1280225
4. Reis GC, Custódio FB, Botelho BG, Guidi LR, Gloria MBA. 2020. Investigation of biologically active amines in some selected edible mushrooms. *J Food Compos Anal* 86: 103375. https://doi.org/10.1016/j.jfca.2019.103375
5. Ficker E, Taglialatela M, Wible BA, Henley CM, Brown AM.1994. Spermine and spermidine as gating molecules for inward rectifier K+ channels. *Science* 266(5187): 1068-1072. https://doi.org/10.1126/science.7973666
6. Morselli E, Mariño G, Bennetzen MV, Eisenberg T, Megalou E, et al. 2011. Spermidine and resveratrol induce autophagy by distinct pathways converging on the acetylproteome. *J Cell Bio* 192(4): 615-629. https://doi.org/10.1083/jcb.201008167
7. Koc E. 2015. Exogenous application of spermidine enhanced tolerance of pepper against *Phytophthora capsici* stress. *Plant Protec Sci* 51(3):127-135. https://doi.org/10.17221/86/2014-PPS
8. Jairath G, Singh PK, Dabur RS, Rani M, Chaudhari M. 2015. Biogenic amines in meat and meat products and its public health significance: a review. *J Food Sci Tech* 52(11): 6835-6846. https://doi.org/10.1007/s13197-015-1860-x
9. Vinci G, Antonelli ML. 2002. Biogenic amines: quality index of freshness in red and white meat. *Food control* 13(8): 519-524. https://doi.org/10.1016/S0956-7135(02)00031-2
10. Weremfo A, Eduafo MK, Gyimah HA, Abassah-Oppong S. 2020. Monitoring the levels of biogenic amines in canned fish products marketed in Ghana. *J Food Quality* 2020: 2684235. https://doi.org/10.1155/2020/2684235
11. Lázaro CA, Conte-Júnior CA, Canto AC, Monteiro MLG, Costa-Lima B, et al. 2015. Biogenic amines as bacterial quality indicators in different poultry meat species. *LWT-Food Sci Tech* 60(1): 15-21. https://doi.org/10.1016/j.lwt.2014.09.025
12. Paulsen P, Bauer F. 2007. Spermine and spermidine concentrations in pork loin as affected by storage, curing and thermal processing. *Euro Food Res Technol* 225(5-6): 921-924. https://doi.org/10.1007/s00217-006-0464-0
13. Til HP, Falke HE, Prinsen MK, Willems MI. 1997. Acute and subacute toxicity of tyramine, spermidine, spermine, putrescine and cadaverine in rats. *Food Chem Toxicol* 35(3-4): 337-348. https://doi.org/10.1016/s0278-6915(97)00121-x
14. Balcerzak W, Pokajewicz K, Wieczorek PP. 2017. A useful procedure for detection of polyamines in biological samples as a potential diagnostic tool in cancer diagnosis. *Applied Cancer Research* 37(1): 23. https://doi.org/10.1186/s41241-017-0032-x
15. Gray N, Plumb RS, Wilson ID, Nicholson JK. 2019. A validated UPLC-MS/MS assay for the quantification of amino acids and biogenic amines in rat urine. *J Chromatogr B* 1106-1067: 50-57. https://doi.org/10.1016/j.jchromb.2018.12.028
16. Angulo MF, Flores M, Aranda M, Henriquez-Aedo K. 2020. Fast and selective method for biogenic amines determination in wines and beers by ultra high-performance liquid chromatography. *Food Chem* 309: 125689. https://doi.org/10.1016/j.foodchem.2019.125689
17. Chow CF. 2020. Biogenic amines-and sulfides-responsive gold nanoparticles for real-time visual detection of raw meat, fish, crustaceans, and preserved meat. *Food Chem* 311: 125908. https://doi.org/10.1016/j.foodchem.2019.125908
18. Munir MA, Badri KH. 2020. The importance of derivatizing reagent in chromatography applications for biogenic amine detection in food and beverages. *J Anal Methods Chem* 2020: 5814389. https://doi.org/10.1155/2020/5814389
19. Ahmad OS, Bedwell TS, Esen C, Garcia-Cruz A, Piletsky SA. 2019. Molecularly imprinted polymers in electrochemical and optical sensors. *Trends Biotechnol* 37(3): 294-309. https://doi.org/10.1016/j.tibtech.2018.08.009
20. Tanima D, Imamura Y, Kawabata T, Tsubaki K. 2009. Development of highly sensitive and selective molecules for detection of spermidine and spermine. *Org Biomol Chem* 7(22): 4689-4694. https://doi.org/10.1039/b909682e
21. Chopra S, Singh A, Venugopalan P, Singh N, Kaur N. 2017. Organic nanoparticles for visual detection of spermidine and spermine in vapors and aqueous phase. *ACS Sustain Chem Eng* 5(2): 1287-1296. https://doi.org/10.1021/acssuschemeng.6b01295
22. Cheng Y, Jiang P, Dong X. 2015. Molecularly imprinted fluorescent chemosensor synthesized using quinoline-modified-β-cyclodextrin as monomer for spermidine recognition. *RSC Adv* 5(68): 55066-55074. https://doi.org/10.1039/C5RA07761C
23. González-Ceballos L, Melero B, Trigo-López M, Vallejos S, Muñoz A, et al. 2020. Functional aromatic polyamides for the preparation of coated fibres as smart labels for the visual detection of biogenic amine vapours and fish spoilage. *Sensor Actuat B-Chem* 304: 127249. https://doi.org/10.1016/j.snb.2019.127249
24. Verma N, Hooda V, Gahlaut A, Gothwal A, Hooda V. 2020. Enzymatic biosensors for the quantification of biogenic amines: a literature update. *Crit Rev Biotechnol* 40(1): 1-14. https://doi.org/10.1080/07388551.2019.1680600

25. Tejpal R, Kumar M, Bhalla V. 2018. Spermidine induced aggregation of terphenyl derivative: an efficient probe for detection of spermidine in living cells. *Sens Actuators B Chem* 258: 841-849. https://doi.org/10.1016/j.snb.2017.11.123

26. Ashley J, Shahbazi MA, Kant K, Chidambara VA, Wolff A, et al. 2017. Molecularly imprinted polymers for sample preparation and biosensing in food analysis: progress and perspectives. *Biosens Bioelectron* 91: 606-615. https://doi.org/10.1016/j.bios.2017.01.018

27. Zhao X, Liu Y, Zuo J, Zhang J, Zhu L, et al. 2017. Rapid and sensitive determination of tartrazine using a molecularly imprinted copolymer modified carbon electrode (MIP-PmDB/PoPD-GCE). *J Electroanal Chem* 785: 90-95. https://doi.org/10.1016/j.jelechem.2016.12.015

28. Zhao X, Hu W, Wang Y, Zhu L, Yang L, et al. 2018. Decoration of graphene with 2-aminoethanethiol functionalized gold nanoparticles for molecular imprinted sensing of erythrosine. *Carbon* 127: 618-626. https://doi.org/10.1016/j.carbon.2017.11.041

29. Alizadeh T, Azizi S. 2016. Graphene/graphite paste electrode incorporated with molecularly imprinted polymer nanoparticles as a novel sensor for differential pulse voltammetry determination of fluoxetine. *Biosens Bioelectron* 81: 198-206. https://doi.org/10.1016/j.bios.2016.02.052

30. Arvand M, Erfanifar Z, Ardaki MS. 2017. A new core@ shell silica-coated magnetic molecular imprinted nanoparticles for selective detection of sunset yellow in food samples. *Food Anal Method* 10(7): 2593-2606. https://doi.org/10.1007/s12161-017-0803-8

31. Silva BV, Rodríguez BA, Sales GF, Maria Del Pilar TS, Dutra RF. 2016. An ultrasensitive human cardiac troponin T graphene screen-printed electrode based on electropolymerized-molecularly imprinted conducting polymer. *Biosens Bioelectron* 77: 978-985. https://doi.org/10.1016/j.bios.2015.10.068

32. Elgrishi N, Rountree KJ, McCarthy BD, Rountree ES, Eisenhart TT. 2017. A practical beginner's guide to cyclic voltammetry. *J Chem Educ* 95(2): 197-206. https://doi.org/10.1021/acs.jchemed.7b00361

33. Fu K, Han D, Ma C, Bohn PW. 2017. Ion selective redox cycling in zero-dimensional nanopore electrode arrays at low ionic strength. *Nanoscale* 9(16): 5164-5171. https://doi.org/10.1039/C7NR00206H

34. Huang YJ, Chang R, Zhu QJ. 2018. Synthesis and characterization of a molecularly imprinted polymer of spermidine and the exploration of its molecular recognition properties. *Polymers (Basel)* 10(12): 1389. https://doi.org/10.3390/polym10121389

35. Zhang J, Wang C, Niu Y, Li S, Luo R. 2017. Electrochemical sensor based on molecularly imprinted composite membrane of poly (o-aminothiophenol) with gold nanoparticles for sensitive determination of herbicide simazine in environmental samples. *Sens Actuators B Chem* 249: 747-755. https://doi.org/10.1016/j.snb.2016.02.068

36. Wang Q, Li S, Li JA. 2018. A molecularly imprinted sensor with enzymatic enhancement of electrochemiluminescence of quantum dots for ultratrace clopyralid determination. *Anal Bioanal Chem* 410(21): 5165-5172. https://doi.org/10.1007/s00216-018-1170-z

37. Emamian S, Lu T, Kruse H, Emamian H. 2019. Exploring nature and predicting strength of hydrogen bonds: a correlation analysis between atoms-in-molecules descriptors, binding energies, and energy components of symmetry-adapted perturbation theory. *J Comput Chem* 40(32): 2868-2881. https://doi.org/10.1002/jcc.26068

38. Frisch MJ, Trucks GW, Schlegel HB, Scuseria GE, Robb MA, et al. 2016. Gaussian 16 Rev. A. 03, Gaussian. Inc., Wallingford, CT, USA.

39. Lu T, Chen F. 2012. Multiwfn: a multifunctional wavefunction analyzer. *J Comput Chem* 33(5): 580-592. https://doi.org/10.1002/jcc.22885

40. Hsu HC, Chen LC, Ho KC. 2004. Colorimetric detection of morphine in a molecularly imprinted polymer using an aqueous mixture of Fe^{3+} and $[Fe(CN)_6]^{3-}$. *Anal Chim Acta* 504(1): 141-147. https://doi.org/10.1016/j.aca.2003.11.021

41. Koklu A, Mansoorifar A, Beskok A. 2019. Effects of electrode size and surface morphology on electrode polarization in physiological buffers. *Electrophoresis* 40(5): 766-775. https://doi.org/10.1002/elps.201800303

42. Khalifa ME, Abdallah AB. 2019. Molecular imprinted polymer based sensor for recognition and determination of profenofos organophosphorous insecticide. *Biosens Bioelectron* X 2: 100027. https://doi.org/10.1016/j.biosx.2019.100027

43. Bossi A, Bonini F, Turner APF, Piletsky SA. 2007. Molecularly imprinted polymers for the recognition of proteins: the state of the art. *Biosens Bioelectron* 22(6): 1131-1137. https://doi.org/10.1016/j.bios.2006.06.023

44. Akhoundian M, Rüter A, Shinde S. 2017. Ultratrace detection of histamine using a molecularly-imprinted polymer-based voltammetric sensor. *Sensors (Basel)* 17(3): 645. https://doi.org/10.3390/s17030645

45. Gao F, Grant E, Lu X. 2015. Determination of histamine in canned tuna by molecularly imprinted polymers-surface enhanced Raman spectroscopy. *Anal Chim Acta* 901: 68-75. https://doi.org/10.1016/j.aca.2015.10.025

46. Ruiz-Capillas C, Herrero AM. 2019. Impact of biogenic amines on food quality and safety. *Foods* 8(2): 62. https://doi.org/10.3390/foods8020062

47. Jiang S, Peng Y, Ning B, Bai J, Liu Y, et al. 2015. Surface plasmon resonance sensor based on molecularly imprinted polymer film for detection of histamine. *Sensor Actuat B Chem* 221: 15-21. https://doi.org/10.1016/j.snb.2015.06.058

48. Cheng Y, Jiang P, Dong XC. 2015. Molecularly imprinted fluorescent chemosensor synthesized using quinoline-modified-β-cyclodextrin as monomer for spermidine recognition. *Rsc Advances* 5(68): 55066-55074. https://doi.org/10.1039/C5RA07761C

49. Kowalska A, Stobiecka A, Wysocki S. 2009. A computational investigation of the interactions between harmane and the functional monomers commonly used in molecular imprinting. *J Mol Struc-Theochem* 901(1-3): 88-95. https://doi.org/10.1016/j.theochem.2009.01.008

50. Xi W, Volkert AA, Boller MC, Haes AJ. 2018. Vibrational frequency shifts for monitoring noncovalent interactions between molecular imprinted polymers and analgesics. *J Phys Chem C* 122(40): 23068-23077. https://doi.org/10.1021/acs.jpcc.8b07771

51. Lefebvre C, Rubez G, Khartabil H, Boisson JC, Contreras-García J, et al. 2017. Accurately extracting the signature of intermolecular interactions present in the NCI plot of the reduced density gradient versus electron density. *Phys Chem Chem Phys* 19(27): 17928-17936. https://doi.org/10.1039/C7CP02110K

52. Huang YJ, Zhu QJ. 2015. Computational modeling and theoretical calculations on the interactions between spermidine and functional monomer (Methacrylic Acid) in a molecularly imprinted polymer. *Journal of Chemistry* 2015: 216983. https://doi.org/10.1155/2015/216983

53. Alkorta I, Legon AC. 2019. Systematic behaviour of electron redistribution on formation of halogen-bonded complexes B···XY, as determined via XY halogen nuclear quadrupole coupling constants. *Phys Chem Chem Phys* 21(31): 16914-16922. https://doi.org/10.1039/C9CP03463C